5-2007

Gamma Ray Burst Afterglow Observations

Adria Updike
Clemson University, aupdike@clemson.edu

GAMMA RAY BURST AFTERGLOW OBSERVATIONS

A Thesis
Presented to
the Graduate School of
Clemson University

In Partial Fulfillment
of the Requirements for the Degree
Master of Science
Physics

---

by
Adria C. Updike
May 2007

Accepted by:
Dr. Dieter H. Hartmann, Committee Chair
Dr. Jeremy R. King
Dr. Sean D. Brittain

ABSTRACT

Gamma ray bursts (GRBs) are among the most luminous explosions in the universe. We present an overview of the observational history of GRBs and the mechanisms involved, then focus on one burst in particular, GRB 070125 and our observational campaign. Finally, we present the results of a model of the global optical response to GRBs, and make recommendations as to how we could improve the global response in preparation for upcoming satellite missions.

DEDICATION

To my parents.

ACKNOWLEDGEMENTS

I would like to acknowledge my committee, Dieter Hartmann, Jeremy King, and Sean Brittain, for their comments and suggestions.

TABLE OF CONTENTS

TABLE OF CONTENTS (Continued)

Page

LIST OF TABLES

LIST OF FIGURES

CHAPTER 1
INTRODUCTION

Gamma-ray bursts (GRBs) are among the most luminous explosions in the universe. Long GRBs ($\sim$ 60 seconds) are believed to be the results of massive stellar collapse, and consist of 'prompt' emission (early emission in the form of gamma rays and immediate optical emission), an afterglow in the x-ray, ultraviolet, optical, near-IR, radio bands, and a supernova emerging a week or so later. Because GRBs have been discovered at distances exceeding those of even quasars (Haislip et al., 2006), they provide a unique tool for probing the (chemical) evolution of the early universe. A burst can, for a brief period of time, act like a flashlight, illuminating the space between itself and us, allowing us to glean information about the structure and composition of the intervening space from their spectra. Therefore, it is important that we continue to improve our observational capabilities in respect to bursts. New satellites and missions will be capable of observing more and higher-redshift bursts, but ground-based observatories must be able to support the larger number of observations needed. In the Science section of this thesis, we examine the capabilities and limitations of current ground-based observatories.

The *Swift* satellite currently localizes about 2 GRBs per week. When a burst is detected, the satellite sends an alert to a list of responders. Automatic telescopes can get on the field within a few seconds to minutes; other telescopes often respond within minutes to hours in an attempt to identify and follow the afterglow emission.

Part of this project consists of a set of programs which determine (based on the time and location of the burst) which telescopes can respond based on the location and magnitude limits of the telescope. We see from this project that we have good coverage of the sky in the R-band, but near-infrared (NIR) bands (J, H, Ks) are lacking. There are R-band capable telescopes situated such that, theoretically, any early burst emission could be observed. As new satellites, such as EXIST and GLAST, begin localizing several bursts a day at higher redshifts, the focus will shift from the optical to the NIR as intergalactic

absorption increases, having more dedicated instruments will become necessary for studying the afterglow decays.

In addition to GRB follow-ups, one burst in particular is studied. GRB 070125 provided a good study of a bright afterglow decay, with a re-brightening around the first day. Our extensive observing campaign is detailed, including observations in the optical, NIR, UV, and x-ray, as well as optical and NIR spectra.

CHAPTER 2
GAMMA RAY BURSTS

GRBs occur either as the result of a massive stellar collapse (long GRB), or as the result of the merging of two neutron stars (short GRB). Long bursts are often associated with the rare type Ib or type Ic supernovae. GRBs are randomly distributed in the sky, implying extragalactic origin, coming from no particular direction, and occur about twice a day.

2.1 Observational History

GRBs were first detected in 1967 by the Vela satellites, placed in orbit by the US to monitor possible infractions of the nuclear test ban treaty. Nuclear tests emit gamma radiation, and since no known sources of gamma radiation beyond nuclear testing and the sun were known, the initial bursts detected were a mystery for many years.

The first satellite aimed specifically at detecting gamma ray emission from extra-planetary sources was the Compton Ray Observatory, which housed the Burst and Transient Source Experiment (BATSE). BASTE provided us with a unique opportunity to study the structure of the gamma ray emission from bursts.

As we can see in Figure 2.4, no two bursts are exactly alike. Bursts range in emission of gamma rays from 10^{-3} to 10^{3} seconds. The shape of the light curves vary significantly from burst to burst. Fortunately, there are other methods for distinguishing bursts.

BATSE detected over 2700 bursts during its nine-year mission. When plotted as a function of T_{90} (the time in which 90% of the gamma ray radiation was recorded), a trend emerges. We see in Figure 2.1 a bimodal distribution of burst durations; the smaller peak of the histogram at ~ 0.3 seconds, and the larger peak at ~ 60 second. This was the first indication that we were dealing with two different classes of GRB.

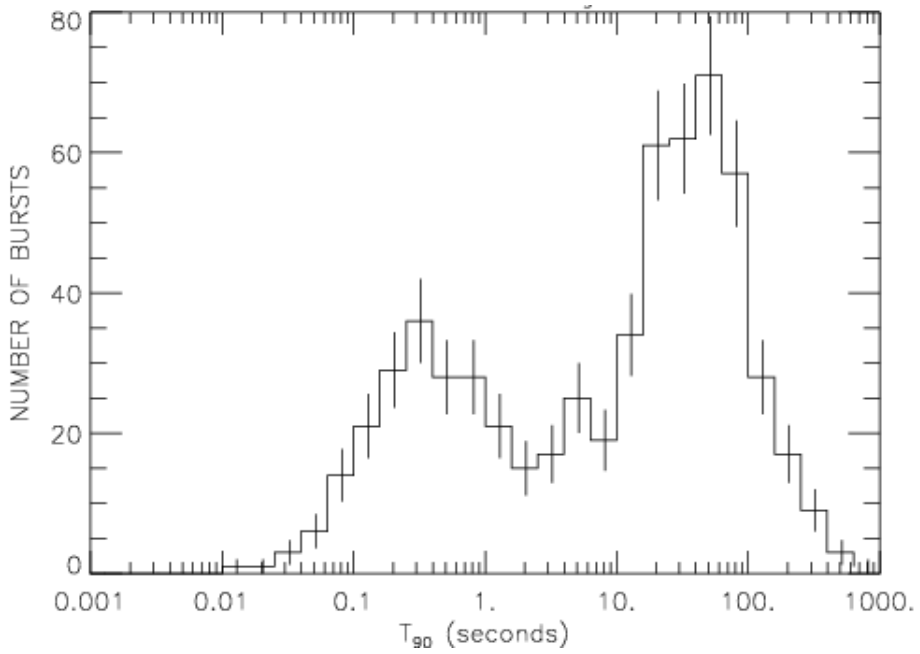

Figure 2.1 Bimodal distribution of GRB timescales as observed by BATSE (Kouveliotou et al., 1993).

The second distinction appears when we plot burst duration vs. the hardness ratio - the fluence from a high energy band divided by the fluence from a lower energy band. This reveals a trend for the shorter duration bursts to have a greater hardness ratio than longer duration bursts (Figure 2.1). The combination of different burst durations and hardnesses led to the conclusion that we were looking at two different mechanisms for a similar observational outcome.

Finally, BATSE gave us our first indication that GRBs are cosmological (extra-galactic) in nature. The bursts were distributed evenly across the sky. If they had originated from a galactic source, the GRBs would have shown up as part of the Milky Way galaxy (Meegan et al., 1992).

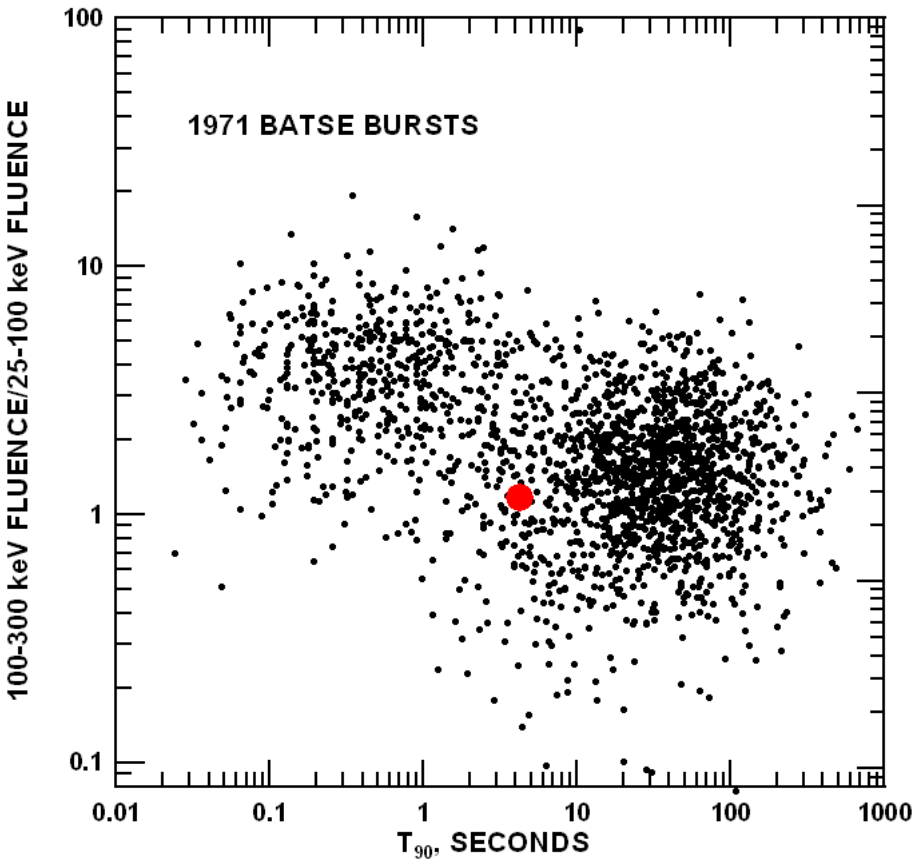

Figure 2.2 BATSE burst durations vs. hardness ratio (**?**).

Gamma ray telescopes use cannot focus the gamma rays, and only indicate a general direction within a degree of the source (Figure 2.1). This does not give an accurate enough position for locating an optical afterglow.

It was not until the Dutch-Italian x-ray and gamma ray satellite Beppo-SAX was launched that we were first able to pinpoint the location of the bursts. When x-ray photons hit a CCD (charge-coupled device) detector, they cause a cascade of electrons, allowing us to get a much better fix on the position (within 3 arc minutes), as well as the energy. Good determination of the position finally allowed for ground-based follow-up. Once ground-based telescopes were capable of following-up on the bursts, spectra of the bursts and host

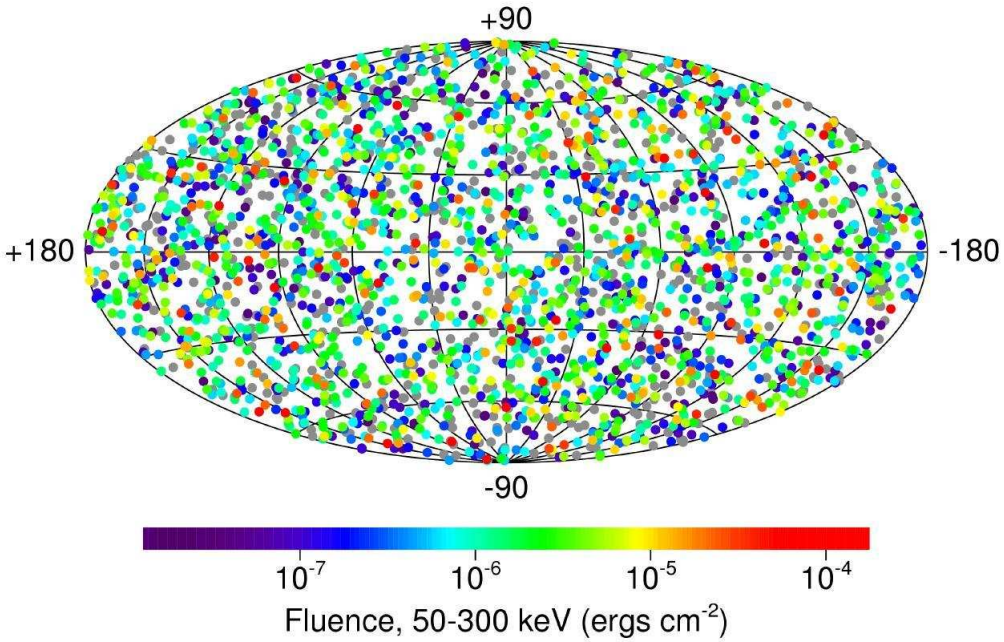

Figure 2.3 Distribution of BATSE bursts on the sky ((Meegan et al., 1996)).

galaxies showed that GRBs were cosmological in nature. These observations provided clear evidence for a model of the emission mechanism known as the 'fireball shock model' (Wijers et al., 1997), one of more than a hundred such models for the observed gamma ray emission.

2.2 Mechanisms

There are three conditions that a star must meet before it is capable of producing a GRB. First, the star must be capable of fusing to iron in its core, which puts a lower mass limit of 40 $M_{\odot}$ (Woosley, 1993). Second, the star must be rotating quickly in order to produce the necessary internal accretion disk to power collimated jets of emission. Finally, it must be of low metalicity for the jets to reach the surface, blowing off the hydrogen envelope as they do so (MacFadyen et al., 2001).

Massive stars are capable of fusing material all the way up to iron. However, when this point is reached, fusion can no longer power the star, and it collapses due to lack of sufficient pressure. As the core of a massive star begins to collapse, a black hole is formed, sending a blast wave through the remaining stellar material at relativistic speeds. When the

blast wave hits the stellar material, gamma rays are produced. This is the first radiation that will arrive at Earth to give us a clue of the explosion.

Following the prompt gamma ray emission, the relativistic collides with gas and dust surrounding the star, emitting photons in the x-ray, ultraviolet, optical, infrared, and radio regimes, which comprise the afterglow of the GRB. The spectral energy distribution is a power-law, as the main source of energy is synchrotron radiation from electrons spiraling around magnetic field lines.

Evidence is strongly in favor of collimated emission, as opposed to isotropic emission. Once it was established that bursts originated at high redshifts (Reichart, 1998), it was realized that if they emitted isotropic, the total energy output in a few seconds, by the gamma rays alone, would be equivalent to the sudden conversion of the entire Sun to energy ($\sim 10^{54}$ ergs) (Rhoads, 1997). If the emission were collimated, or concentrated along a jet rather than isotropically, the energy needed would be significantly reduced (on the order of 10^{50} ergs).

When the center of the massive, collapsing star forms a black hole, an accretion disk will form inside the star. As the accretion disk falls into the black hole, it fuels a set of jets along the rotation axis of the star. The matter density here is much lower than around the equator where the disk is forming.

2.3 Prompt Emission and Afterglow Behavior

The jet leaving the star is not a smooth stream of material, but rather a series of shock waves moving at relativistic speeds. As the outer shells reach the exterior of the star, they are slowed as they encounter the interstellar medium, and the shells behind them collide with the outermost shells, dissipating energy as they slow down and emitting the energy as gamma radiation. This is the source of the initial burst of gamma rays.

As additional shocks catch up to the initial slowed shock, they collide in short bursts of energy known as prompt emission. They cause rapid flaring events seen in the x-ray through infrared bands. These initial shock collisions are brief in nature and do not appear to occur after the first few hundred seconds after the gamma ray emission, with some notable exceptions.

The gamma rays emitted by the burst are non-thermal photons in the MeV range, but sometimes extend into the GeV range. As interstellar matter encounters the shock wave, it is superheated. These particles, now moving at relativistic speeds, emit synchrotron radiation as they encounter magnetic fields. The bulk of the afterglow flux is emitted by electrons generated in the shock region.

The best evidence for jet collimation comes from the observance of a break in the light curves of afterglows, usually a few days after detection. If the radiation from the GRB is being emitted in a highly-relativistic jet in the direction of Earth, the initial emission will be 'beamed' towards us according to special relativity. As the jet slows in the external medium, the bulk Lorentz factor of the material decreases until it reaches $1/\theta_b$ (the geometric angle of the jetted outflow). At this point, we are seeing the entire 'beamed' cone of radiation. This is known as the 'jet break'.

Other features, besides the jet break, can occur as well. Optical flashes have been observed in several bursts (e.g. (Akerlof et al., 1999)). These flashes are usually attributed to a reverse shock propagating back through the ejecta.

A curious class of bursts known as 'dark bursts' have been observed, where there is no apparent afterglow. Although nearly half of the bursts observed by Swift have no accompanying afterglow, this may be due to the extreme redshift of the burst. High-redshift bursts are shifted entirely into the near-IR if they do have an afterglow Figure 5.2, but recent near-IR observations of 'dark bursts' often yield nothing, such as in the case of Updike et al. (2007b).

2.4 Resulting Supernovae

In 1998, the first GRB with an accompanying supernova was detected (Bloom et al., 1999). The burst was 980425, a dark burst, and the resulting supernova, 1998bw, has been used as a template for many burst-related supernova. However, the lack of an optical afterglow cast doubt on whether or not GRB 980326 was actually related to SN 1998bw, or simply coincident. The discovery of GRB 030329 with a bright optical afterglow and SN 2003dh firmly established the GRB / SN connection (Stanek et al., 2003). SN 1998bw has since been shown to be over-luminous in comparison to other GRB-selected supernova.

There are several recognized types of supernova. They were originally divided into two types, Type I and Type II. Type I had no visible hydrogen lines, and Type II contained hydrogen lines. They were further subdivided into Type Ia, Type Ib, and Type Ic. Type Ib supernova are notable for having a strong non-ionized helium line and no silicon absorption features, where as the type Ic has few to no helium lines and no silicon features. However, the division was misleading, as it turns out that Type Ia supernova are caused by the accretion of matter onto a White Dwarf from a companion star until the Chandrasekhar limit of 1.44 solar masses has been reached and it explodes, unlike Type Ib, Ic, and Type II supernova, which are caused by the core collapse of a massive star. GRBs are associated with the rare Type Ib and Ic supernova.

Using 1998bw as a template, we can predict the luminosity of emerging supernova. However, several GRBs were recently shown not to have a supernova (Fynbo et al., 2006), so it seems likely that there is a yet-misunderstood category.

2.5 Host Galaxies

Studies of GRB host galaxies tend to reveal small, blue irregular galaxies as hosts (Fruchter et al., 1999). In addition, the galaxies tend to be of low metallicity (as expected from luminosity-metalicity relationships). In fact, low metallicity may be a requirement for the creation of a GRB, since stars with high metallicity have stronger stellar winds, which are more likely to reduce the overall angular momentum of the star. As the winds are ejected from the star, they apply a torque to the star by coupling to the its magnetic field. This spins down the star and makes jet formation less likely Matt & Pudritz (2005). Because the angular momentum plays a significant role in the formation of the jets via an accretion disk, it is likely that a high metallicity star (from a high metallicity galaxy) is less likely to produce a burst.

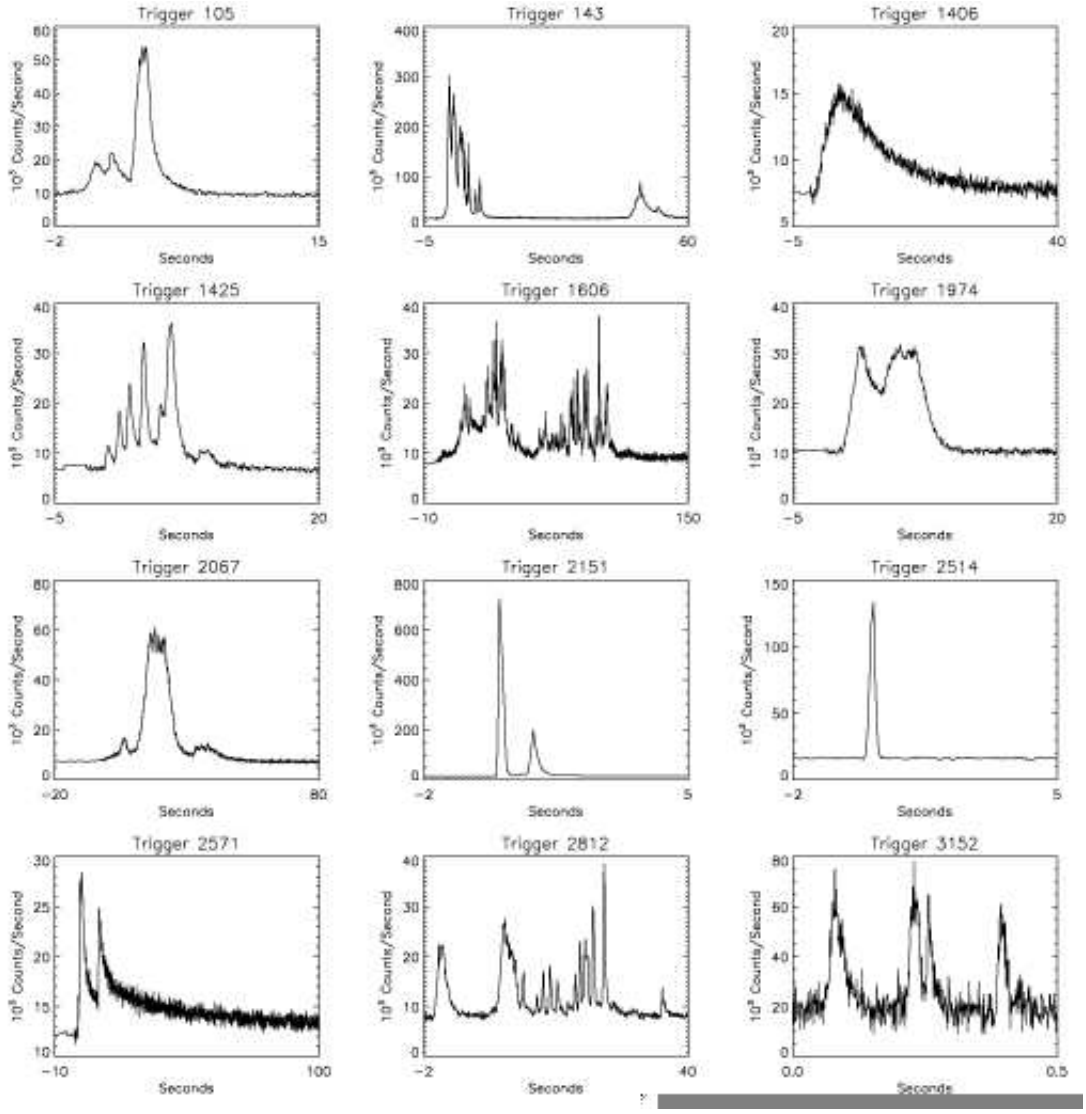

Figure 2.4 GRB profiles in the gamma ray regime as observed by BATSE (Fishman & Meegan, 1995).

CHAPTER 3
AFTERGLOW OBSERVATIONS

GRB afterglows have been detected in the optical, near-IR, ultraviolet, x-ray, and radio wavelengths, in addition to gamma ray 'tails'. In this section, we discuss several of the instruments aiding in detection and follow-up observations.

3.1 Space-Based Instrumentation and Follow-Up

3.1.1 *Swift*

Swift[1] is a multi-wavelength satellite containing optical, ultraviolet (UVOT), x-ray (XRT), and gamma ray (BAT) detectors launched by NASA. It's mission objectives include localizing GRBs, as well as studying GRBs and supernova in multi-wavelengths. Launched November 20, 2004, it detects about 2 GRBs per week.

The BAT telescope on-board *Swift* has a field of view covering approximately one sixth of the sky. Upon discovery of a burst, the XRT can quickly determine an accurate position (error circle of 3 arc minutes). This inclusion of an x-ray positioning telescope was an essential improvement over earlier methods, which often took hours to localize a burst, by which time many have faded beyond the reach of ground-based observatories.

When a burst is localized, the position is sent to scientists and telescopes all over the world through the GCN network to enable rapid follow-up of bursts. Our response team has limited access to several telescopes, including SARA, Super-LOTIS, and the Mayall 4m.

3.1.2 Additional Current Space-Based Missions

In addition to *Swift*, there are several other satellites that can detect GRBs. The *High Energy Transient Explorer* (HETE 2)and the *Rossi X-ray Timing Explorer* (RXTE) also contribute to burst identification. The *InterPlanetary gamma-ray timing Networks* (IPN) and Integral are also responsible for burst detection and localization.

---

[1] http://swift.gsfc.nasa.gov

HETE 2 was launched in 2000 after the original HETE was destroyed in deployment in 1996. It was instrumental in establishing the connection between GRBs and supernova, as well detecting the first short, hard burst for which an optical afterglow was discovered.

3.1.3 GLAST

The *Gamma ray Large Area Space Telescope*[2] (GLAST) is a NASA project aimed at studying high-energy gamma rays. It is expected to launch in 2007. Among its stated mission objectives is to study the high-energy behavior of gamma ray bursts.

GLAST has a field of view of about 2.5 sr, or about 20% of the sky. The GLAST Burst Monitor will be able to detect and localize gamma ray bursts, as it is sensitive to the high-energy x-ray regime as well as gamma rays. Due to its smaller field of view, GLAST should be able to detect one to two GRBs per week.

3.1.4 EXIST

The *Energetic X-ray Imaging Survey Telescope*[3] (EXIST) will include x-ray and gamma ray detection capabilities in order to localize and study gamma ray bursts as its primary mission objective. Its wide field of view (allowing it to image the entire sky every 90 minutes) affords it unprecedented coverage of the sky as compared to earlier instruments, and its improved sensitivity over the *Swift* satellite will allow it to detect 2 - 3 GRBs per day.

EXIST will be capable of detecting bursts in a range largely unexplored by current instruments, namely z in the 6 - 20 range. The furthest burst detected by *Swift* was z=6.24.

3.1.5 HST

The Hubble Space Telescope[4] (HST) was launched in 1990. It has been an invaluable tool for studying the optical afterglows of GRBs because it is capable of obtaining a

[2] http://www-glast.stanford.edu

[3] http://exist.gsfc.nasa.gov

[4] http://hubble.nasa.gov/index.php

higher-resolution image than ground-based observatories (which are limited in resolution by the atmosphere).

The first burst observed by Hubble was GRB 990123, providing clear evidence for a jet break in the light curve and lending credence to arguments for relativistic beaming ((Fruchter et al., 1999)).

3.1.6 JWST

The *James Webb Space Telescope*[5] (JWST) is NASA's successor to the Hubble Space Telescope, scheduled for launch in 2013. It will contain infrared imaging and spectroscopes, that will optimize its use for detecting high-redshift bursts (see Figure 5.2).

JWST will be an essential instrument to aid in the follow-up of high-redshift bursts. As we see in Figure 5.2, the emission of bursts at higher redshifts does not extend into the optical regime, but rather fall out earlier, extending only so far as the near-infrared. Many ground-based observatories lack infrared capabilities, so having an instrument in space that can follow-up in deep imaging and spectroscopy will greatly aid in the detection and redshift determinations of bursts and their host galaxies.

3.2 Ground-Based Instruments

As we will see in Section 5, there are observatories all over the world assisting in ground-based follow-up to GRBs. We will discuss several specific instruments that our response team has utilized in the search for afterglows.

3.2.1 Optical Imaging with Super-LOTIS

Super-LOTIS[6] is a robotic 0.6 meter telescope located on Kitt Peak, Arizona. Its primary mission is to observe the prompt (early) afterglow emission, as well as observing the resulting supernova (see Section 2.4). Super-LOTIS's small size allows it to rapidly slew to a burst field and begin imaging within seconds of a burst detection by *Swift*. Super-LOTIS

[5] http://www.jwst.nasa.gov

[6] http://slotis.kpno.noao.edu/LOTIS

can reach a limiting magnitude of 18.5 in the R-band in a single 60-second exposure, making it an ideal instrument to observe prompt emission and resulting supernova. Dedicated instruments such as Super-LOTIS provide much-needed information on bursts. The selling points of Super-LOTIS are its quick response time, accurate pointing, Landolt photometry (standard fields used for photometric calibration), four filters, and automatic image reduction and alignment, needing a minimum amount of user support. The Clemson support for Super-LOTIS involves running the nightly set-up tasks once a week, monitoring the GCNs for a burst, and reducing the data from a burst to send out a GCN notice on any results.

3.2.2 Optical Imaging with SARA

Clemson is a member of the *Southeastern Association for Research in Astronomy*[7] telescope (SARA), which is also located on Kitt Peak. SARA is a 0.9 meter Cassegrain telescope, which is controlled remotely by members of the SARA consortium. The Clemson group requests less scheduled time on the telescope in exchange for target of opportunity (ToO) time to observe GRBs.

As a larger instrument than Super-LOTIS, SARA can observe objects down to 21 magnitudes in the R-band in about an hour's worth of stacked images. A series of reduction routines (Garimella, 2005) have been written to automatically reduce, align, and stack the SARA images.

3.2.3 Near-IR Observations using FLAMINGOS

The *Florida Multi-object Imaging Near-IR Grism Observational Spectrometer*[8] (FLAMINGOS) is a near-IR imager and spectrograph, commissioned in 2001, currently in use at Kitt Peak. As a result of the NOAO-Clemson collaboration, our group has used FLAMINGOS on the 2- and 4-meter telescopes on Kitt Peak.

FLAMINGOS supports observations in the J, H, and K bands, as well as spectroscopy. The limiting magnitude in the J-band after an hour's worth of imaging is about 21 magnitudes, making FLAMINGOS an ideal instrument for studying higher-redshift bursts.

---

[7] http://astro.fit.edu/sara/sara.html

[8] http://www.noao.edu/kpno/manuals/flmn/flmn.html

Near-IR image reduction requires subtracting the high sky background. Our reduction was done using the ECLIPSE package (Devillard, 1999). The ECLIPSE package does the flat-fielding and dark subtraction, as well as alignment and reduction of the sky background on dithered NIR images.

3.3 Redshifts

Determining the redshift of a burst is particularly useful. We are mainly interested in long GRBs, or those which are best modeled by the collapse of an extremely massive star. These massive stars existed exclusively in the beginning of the universe, and obtaining spectra of them can lead to a wealth of information about the structure and composition of the early universe. Early determination of the redshift encourages follow-up in the optical regime for interesting, high-redshift bursts. Therefore, it is in our best interests to obtain a redshift quickly.

3.3.1 Spectroscopic

Spectroscopy, in the optical and near-IR, is the most accurate method for determining GRB redshifts. Because GRBs are cosmological in nature, they will show up as the most-redshifted objects in the spectrum. Intermediate galaxies can also be identified based on the existence of a Lyman-α forest and/or absorption and emission features, such as silicon or magnesium.

3.3.2 Photometric

Redshifts determined not from spectra, but through examination of the spectral energy distribution (SED) are divided into two categories - photometric redshifts and pseudo-redshifts.

Photometric redshifts can be obtained by measuring the relative SEDs several filters, and plotting the flux vs. wavelength to see where the bands begin dropping out (Figure 5.2).

Pseudo-redshifts are determined based on the parameters of the prompt emission using the Amati correlations (Amati, 2005).

These methods can prove useful for determining the approximate redshift of bursts for which no spectrum can be obtained. Although they are not as accurate as spectra, they are more easily obtained for high-redshift bursts due to the faint nature of the sources.

CHAPTER 4

GRB 070125

4.1 Observational Campaign

GRB 070125 was localized by RHESSI (Hurley et al., 2007) on Jan 25, 2007, at 07:20:42 UT. The IPN-BAT localization was sent at 21:46:48 UT, at which point ground-based observations began. The burst was described as a long (approximately 60 seconds), intense burst. An afterglow candidate was identified by the 60 inch Palomar telescope (Cenko & Fox, 2007) on Jan 26, 2007 at 03:30:35 UT, and confirmed by the SARA telescope (Updike et al., 2007a) at 04:41:53 UT. Further observations were carried out by Xinglong (Xing et al., 2007), SWIFT/UVOT (Marshall & Racusin, 2007), KANATA (Uemura et al., 2007), PROMPT (Haislip et al., 2007), Loiano (Greco et al., 2007), AAVSO (Durig, 2007), MITSuME (Yoshida et al., 2007), PAIRITEL (Bloom et al., 2007), and at the Bok and Kuiper telescopes by Peter Milne. These observations were carried out within the 11 days following the trigger. An additional detection was made at the Large Binocular Telescope (LBT) 26.8 days after the burst (Garnavich et al., 2007).

A spectrum of the burst was obtained on Jan 26, 2007 using the Gemini North telescope+GMOS (Fox et al., 2007), approximately 23 hours after the burst. Earlier spectra from the Lick 3m (Prochaska et al., 2007a) and Keck-I (Prochaska et al., 2007b) showed a curious lack of prominent absorption features, leading the observers to a low-z conclusion. However, the Gemini spectrum revealed the presence of a single, weak absorption doublet located at observer-frame wavelengths of 7122.9 Å+ 7140.9 Å, identified as Mg II, placing the GRB at z=1.547. This information was released on Feb 3, 2007.

GRB 070125 remained bright enough to be detectable by 2 - 4m class telescopes for 3 to 4 days after the burst was localized. After it had faded beyond their capabilities, several instruments continued observations (SARA, Kuiper) in the hopes of observing the supernova-related re-brightening, as the GRB was initially thought to have occurred at low z. Models of the standard SN 1998bw thus predicted a bright supernova within a week of

the burst. However, no supernova was detected. The reason for this was clear upon the announcement of a redshift of 1.547. Further modeling, accounting for redshift, now predict a supernova peak brightness of R = 27.0, J = 24.4 magnitudes 30 days after the burst.

4.2 SARA Response

Based on the GCN reports, SARA was the first telescope to respond to GRB 070125. Although we have the earliest data, high airmass, malfunctioning mirror covers, and degrading focus led to a large amount of scatter in our individual data points. We were able to reduce the scatter by binning the data in blocks of an hour to an hour and a half.

SARA observations were conducted in the V band. SARA detected the afterglow for three days after the GCN notice. Due to the fact that the IPN notice was sent out nearly a day after the burst was detected, there is no observed prompt emission.

4.3 Light Curve Fitting

We have extensive light curves covering the first four days after GRB 070125. To obtain a power-law decay fit, we began by fitting a Beuermann function (Beuermann et al., 1999).

$$f = \left(f_1^{-\alpha_1} - f_2^{-\alpha_2}\right)^{\frac{-1}{n}} \tag{4.1}$$

Further refinements to the Beuermann function resulted in the Rhoads & Fruchter function, which we employed to fit our light curves. The initial decay rate is α_1, the decay rate after the jet break is α_2, t_b is the jet break time, t is the time in days, $F_\nu(t_b)$ is the flux at the time of the jet break, and n is the sharpness of the curve at the jet break time.

$$f_\nu = 2^{\frac{1}{n}} F_\nu(t_b) \left[\left(\frac{t}{t_b}\right)^{\alpha_1 n} + \left(\frac{t}{t_b}\right)^{\alpha_2 n}\right]^{\frac{-1}{n}} \tag{4.2}$$

We used a least-squares method to fit the function to the R-band data. Our best-fit results are shown in Figure 4.3. The fluxes have been converted to magnitudes.

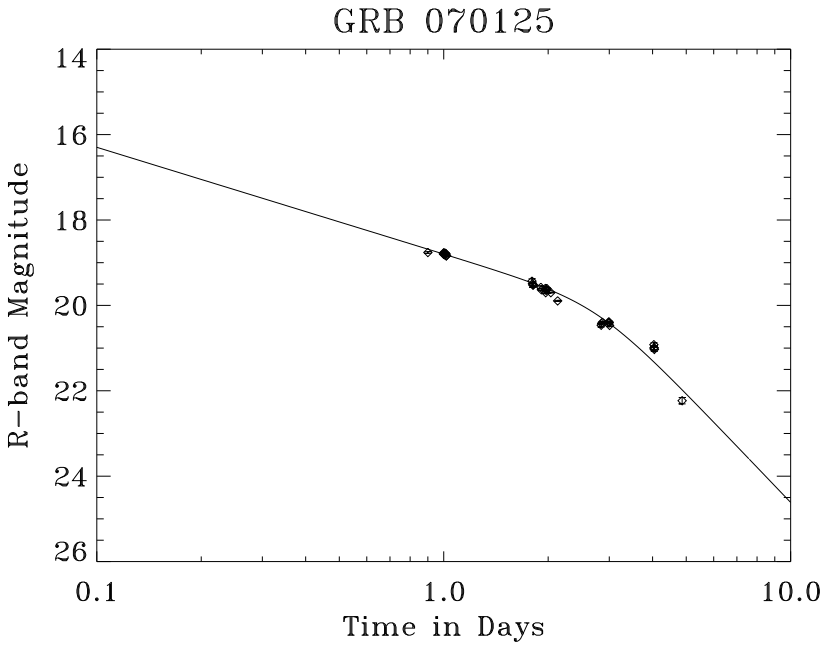

Figure 4.1 Broken power-law decay fit to the R-band data.

Our fit results give us an initial decay rate of $\alpha_1 = 1.2$, a final decay rate of $\alpha_2 = 3.8$, a jet break time of 3.5 days, and a $n = 2.25$. The flux at the time of the jet break was 5.012×10^{-9} photons/cm^2/second. The reduced chi-squared value for this fit was 0.022.

The R-band observation carried out at the LBT at 26.8 days revealed a source at the position of the afterglow at 26.3 ± 0.3 magnitudes. There are three main ways to interpret this data point. First, we could be witnessing a late-time re-brightening of the afterglow. However, this is not likely, as current models would predict that there is not enough left of the star at this point to fuel a re-brightening. A second possibility, and the most likely, is that the LBT has detected the host galaxy.

If this is indeed the host galaxy, we would like to measure its luminosity. First, we need to determine the expansion rate as a function of redshift.

$$E^2 = \Omega(1+z)^3 + \Omega_R(1+z)^2 + \Omega_\Lambda \tag{4.3}$$

In Equation 4.3, Ω is the density parameter of the universe (taken to be 0.3), Ω_R is the curvature parameter (taken to be 0), and Ω_Λ is the cosmological constant (taken to be 0.7 (**?**)). For our host galaxy redshift of 1.547, this gives us an expansion coefficient of 2.378.

From this, we can calculate the cosmological correction $y(z)$ to the luminosity distance equation d_L.

$$y(z) = \int_0^{1.547} dz' E^{-1}(z') = 0.662 \tag{4.4}$$

The luminosity distance is calculated as

$$d_L = \left(\frac{c}{H_0}\right)(1+z)y(z) = 7025 Mpc \tag{4.5}$$

taking the value of the Hubble constant H_0 to be 72 $km/s/Mpc$ (Melchiorri & Ödman, 2003). When we evaluate this at our redshift of 1.547, we calculate a luminosity distance of 7025 Mpc. Now we can use our d_L to measure the absolute magnitude of our host galaxy.

$$M = m + 5 - 5log(d_L) \tag{4.6}$$

The apparent magnitude is 26.3 as measured by the LBT, and our value of d_L has been converted to parsecs. This gives us an absolute magnitude of -17.9 for our host galaxy. When we compare this to the absolute magnitude of our Milky Way galaxy (-20.5), we see that our host galaxy is much dimmer. This follows the general trend for GRB host galaxies to be dimmer on average than our own galaxy and even most galaxies found at a similar epoch (Wolf & Podsiadlowski, 2007).

A third possible interpretation of the LBT data point is the emergence of a supernova. Based on models of supernova 1998bw, Sylvio Klose has provided us with a prediction of the resulting supernova in the R-band at z=1.547. If we shift the predicted supernova 'bump' up to the position of the last data point obtained by the LBT (Figure 4.2, we would find that is this IS the resulting supernova, it would be 1.69 $\pm$ 0.27 times as luminous as 1998bw. This luminosity difference was obtained by taking the peak flux as predicted by

the model for SN 1998bw and multiplying it by 1.69 to get it up to the brightness predicted by the LBT point. This was then converted back into magnitudes from fluxes for the plot. However, this is a point of some contention. Most GRB-selected supernova are in fact dimmer than SN 1998bw. In addition, if this were indeed the emerging supernova, it would be the furthest core-collapse supernova ever detected.

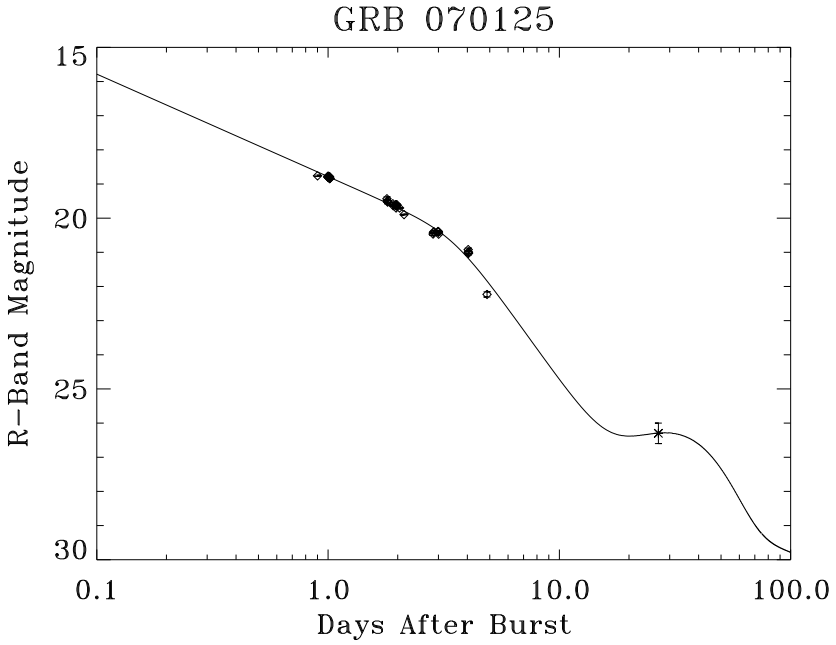

Figure 4.2 R-band light curve with broken power-law fit and resulting supernova.

In order to determine if we are observing a supernova or the host galaxy, we attempted to get one more observation done on the target. If the magnitude remains in the ballpark of 26.3, then we have most likely detected the host galaxy. If the magnitude has dropped significantly or the target is no longer visible, then we did indeed detect the supernova. However, as our Hubble proposal was unsuccessful, we must conclude that we are indeed observing the host galaxy.

4.4 Mechanics

Finally, we wish to calculate the overall energy output of GRB 070125. Using the luminosity distance calculated in Equation 4.5 and the fluence (time integrated flux) reported by the RHESSI team (Bellm et al., 2007) of 1.5×10^{-4} erg/cm^2 in the 30 keV to 10 MeV range. The energy emitted in the GRB, if it had been isotropically emitted, can be calculated as

$$E_{iso} = 4\pi S d_L^2 (1+z)^{-1} \tag{4.7}$$

to be 3.79×10^{53} ergs. However, we know that the energy is emitted in collimated jets. We can calculate the jet opening angle (Sari et al., 1999)

$$\theta_j = 0.057 \left(\frac{t_j}{1day}\right)^{\frac{3}{8}} \left(\frac{1+z}{2}\right)^{-\frac{3}{8}} \left(\frac{E_{iso,\gamma}}{10^{53} ergs}\right)^{-\frac{1}{8}} \left(\frac{\eta_\gamma}{0.2}\right)^{\frac{1}{8}} \left(\frac{n}{0.1 cm^{-3}}\right)^{\frac{1}{8}}, \tag{4.8}$$

where t_j is the jet break time, η_γ is the efficiency of the shocks at converting the collision energy into gamma rays, and n is the density of the exterior medium, taken to be the density of interstellar hydrogen. η_γ is taken to be 0.2 (Guetta et al., 2001). This gives us a jet opening angle of 0.094 radians (5.4 degrees). We can now calculate the energy emitted in collimated emission (Frail et al., 2001)

$$E_\gamma \simeq \frac{\theta_j^2}{2} E_{iso,\gamma}. \tag{4.9}$$

This gives us a corrected GRB energy output of 1.67×10^{51} ergs. Figures 4.3 and 4.4 show us that the opening angle of GRB 070125 and energy output are consistent with previously observed bursts.

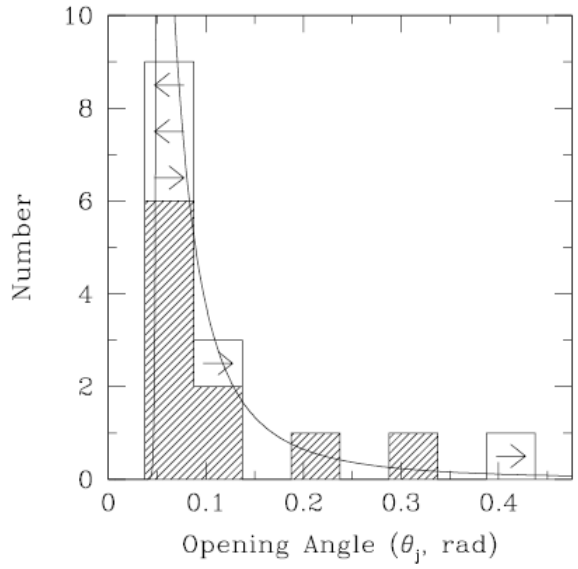

Figure 4.3 Observed distribution of jet opening angles with fit line (Frail et al., 2001).

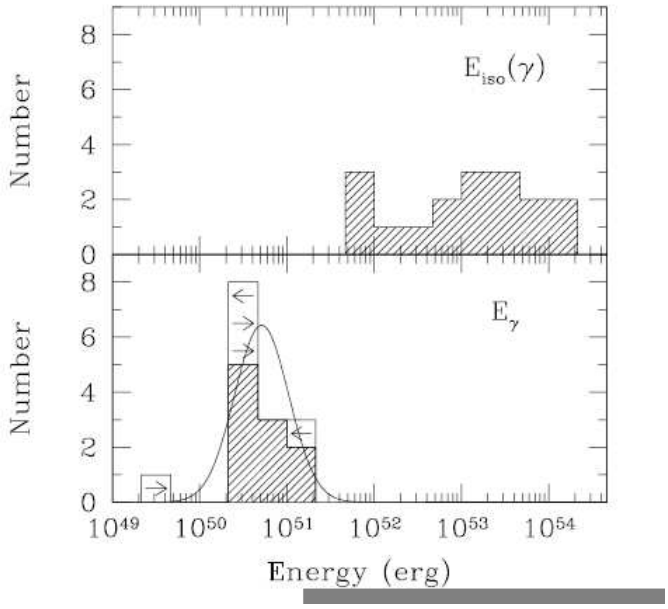

Figure 4.4 The distribution of isotropic energies for bursts with known redshifts (top) and the energy emitted in jets for the same bursts (bottom). Note that the energy distribution is much smaller once the collimation correction has been applied (Frail et al., 2001).

CHAPTER 5
MODELING THE GRB RESPONSE NETWORK

In this section, we will discuss a model of the current global GRB response network (Updike et al., 2006).

5.1 Goals

The goal of this project was to determine the global optical and NIR response to GRB afterglows. This allows us to predict which instruments would be capable of responding to a burst at some given position in the sky. This information will prove useful in the future as upcoming satellites will be capable of identifying many more bursts and at scientifically interesting higher redshifts.

5.2 Current and Future Satellites

The SWIFT satellite currently localizes about two bursts per week, the majority of which are relatively low redshift ($z < 3$, see Figure 5.1).

Upcoming satellites, such as EXIST and GLAST, are predicted to locate two bursts per day. Currently, there are a number of telescopes that respond automatically to GRBs (ROTSE, RAPTOR, Super-LOTIS, KAIT, PROMPT, etc). These are typically small instruments that are aimed at seeing the prompt emission, and as such, do not have to have large mirrors, since prompt emission in the optical bands for low-z bursts is usually in the 13 to 18 magnitude range. Follow-up at later times can be done by the larger instruments that require either scheduled time or target of opportunity observations.

However, EXIST will be capable of localizing bursts at higher redshifts ($z > 10$). These bursts will be necessarily dimmer than burst at lower redshifts, and thus the smaller, robotic telescopes may not be capable of detecting them (see figure: make figure on how redshift affects magnitude). As we can see in Figure 5.2, as the redshift increases, certain bands drop out - the burst is no longer visible in those bands.

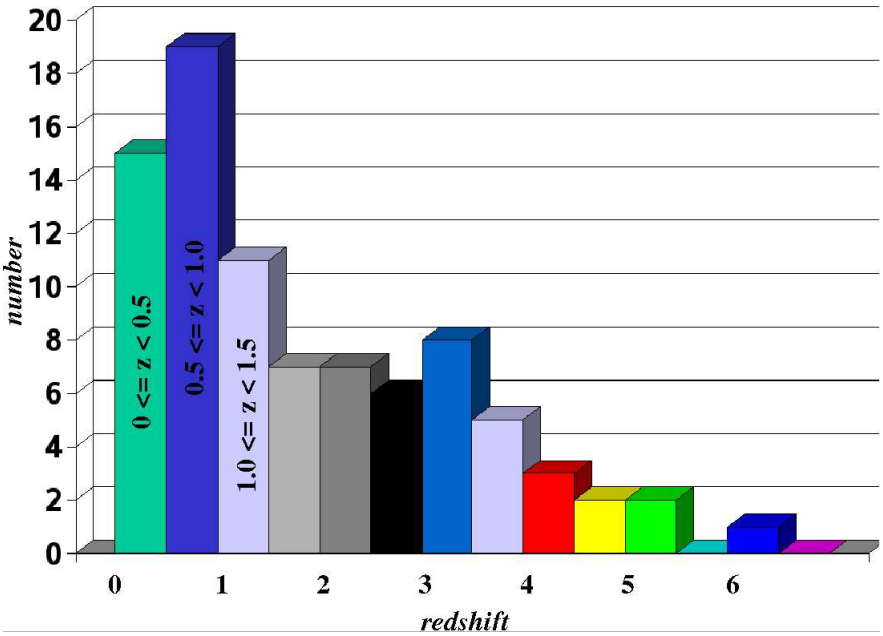

Figure 5.1 Bursts detected with Swift as a function of redshift.

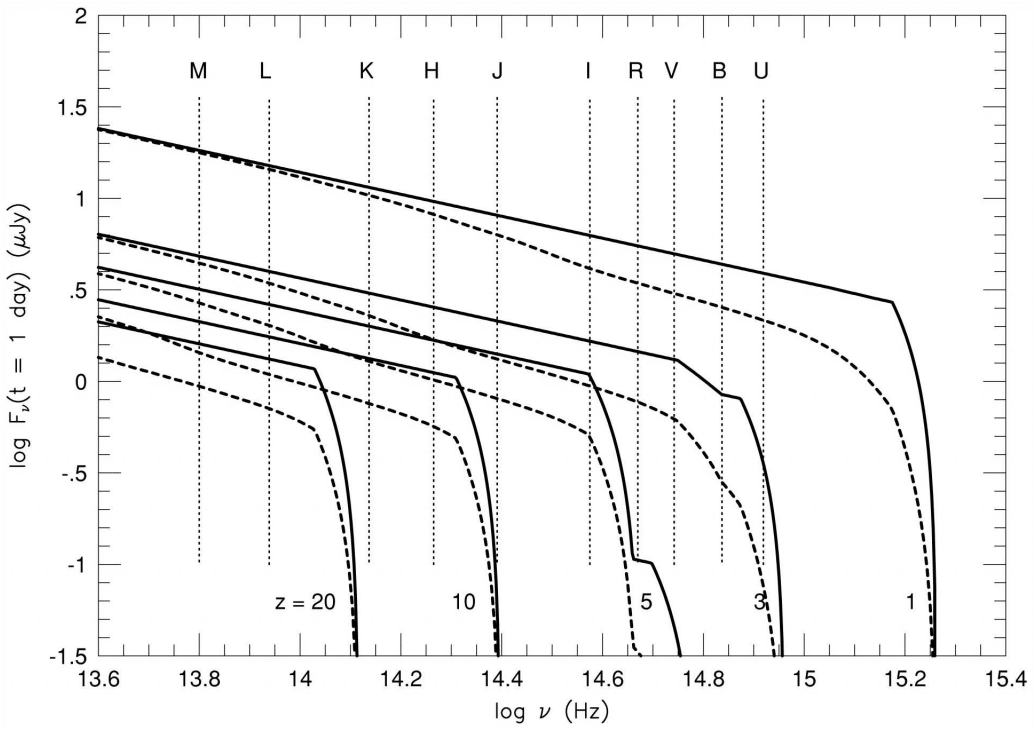

Figure 5.2 Afterglow dimming as a function of redshift. (Lamb & Reichart, 2001).

Higher redshift bursts will be detectable in the NIR, which means we will require more robotic NIR instruments in order to get anywhere near the same kind of coverage we can get of GRBs now when we are relying on the new instruments. In addition, relying on larger instruments to establish the light curve after a few hours will be much harder when we are finding two burst per day vs. two per week, because time on these telescopes is limited. More dedicated NIR instruments, both at the robotic and larger sizes, must be made available in order to continue observing GRBs.

5.2.1 Telescopes and Rankings

In order to determine the global optical response, GCNs were analyzed over a period of a year (December 25, 2005 to December 26, 2006). Over a hundred and twenty telescopes responded to GRBs during that period. Of these, the top 30 instruments were identified based on the number of bursts they responded to and reported via a GCN.

Table 5.1. Top Responding Telescopes

Telescope	Rank	PM	Lat	Long	GCNs	Band
VLT	1	8.2m	-24.626	-70.403	30	R
Miyazaki	2	1.5m	31.899	131.433	23	R
NOT	3	2.5m	28.757	-17.885	22	R/J
SkyNet	4	0.41m	-30.169	-70.806	21	R,V,I
Palomar 60	6	1.52m	33.356	-116.866	17	R
MAO	5	1.5m	38.683	66.933	20	R clear
REM/ROSS	6	0.6m	-29.255	-70.738	17	R/J
MDM	6	1.3/2.4m	31.98	-111.6	17	R
Gemini S	6	8.1m	-30.169	-70.717	17	R
TAROT	6	0.25m	-29.26	-70.738	17	R
Faulkes N	7	2m	20.713	156.258	14	R
Xinglong	7	0.8m	40.39	-65.425	14	R
CTIO	7	1.3m	-30.169	-70.806	14	R
Liverpool	7	2m	28.757	-17.885	14	R
Tubitak	7	1.5m	36.825	2.022	14	R
Super-LOTIS	8	0.6m	31.98	-111.6	11	R
MASTER	8	0.2m	37.810	55.381	11	clear
Keck I/II	8	10m	19.817	-155.467	11	R
Bootes	9	0.6m	37.1	6.7	9	R/J
Loiano	10	1.52m	44.258	11.337	6	R
WATCHER	10	0.4m	-29.042	26.397	6	R
OPTIMA	10	1.3m	26.211	24.899	6	R/J
SARA	11	0.9m	31.98	-111.6	5	R

Table 5.1 (cont'd)

Telescope	Rank	PM	Lat	Long	GCNs	Band
ROTSE IIIa	11	0.45m	31.277	149.066	5	R
Lulin	11	1m	25	121	5	R
PAIRITEL	11	1.3m	31.688	-110.884	5	J
Tautenburg	11	1.34m	50.983	11.717	5	R
FRAM	12	0.2m	-35.2	-69.2	4	R
Dan Tel	12	1.5m	-29.254	-70.735	4	R
ART	12	0.35m	34.786	135.438	4	R
MITSuME	12	0.5m	34.5	136.7	4	clear
Faulkes S	13	2.0m	-31.277	149.066	3	R
KAIT	13	0.76m	37.343	-121.534	3	R

5.2.2 Visibility

The visibility of a burst for a particular instrument was determined from the RA and Dec of the burst, as well as the location of the instrument. In addition, observational constraints such as the bands available and the magnitude limit of the telescope were considered.

The program ALT.PRO (Updike, 2006) calculates the altitude and visibility of a GRB at a given date and time for a given instrument. Using this information, we were able to determine which telescopes could theoretically respond to a given burst, given good weather conditions and no instrument trouble. This lead to a second set of rankings based on how often a telescope responded to and published a GCN on bursts that they were capable of detecting.

We would expect this set of rankings to favor the smaller, robotic telescopes, since the larger telescopes often require scheduled time or target of opportunity observations. However, we see that one of our top ranking telescopes is the VLT.

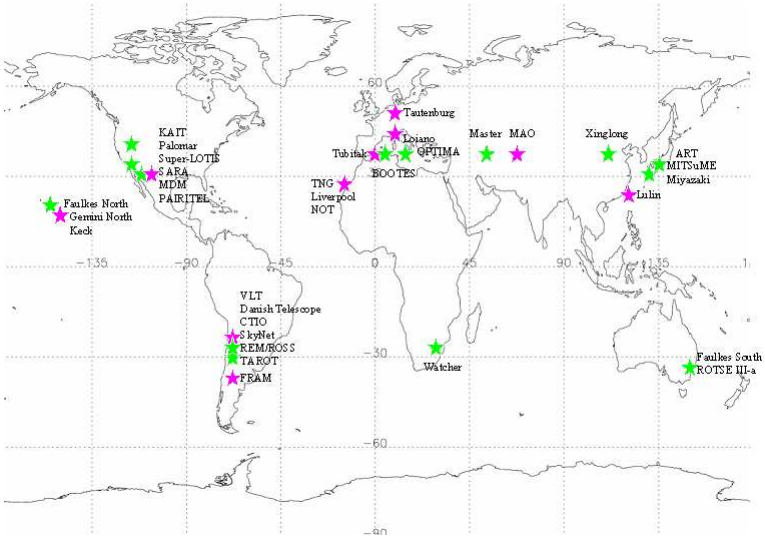

Figure 5.3 Map of the locations of the top 30 responding telescopes. Green stars represent robotic telescopes.

Table 5.2. Instrument Response

Telescope	Response
REM/ROSS	67%
VLT	58%
Miyazaki	56%
Super-LOTIS	46%
CTIO/SMARTS	40%
Nordic Optical Telescope	40%
SkyNet (PROMPT)	38%
FRAM	33%
TAROT	33%
Faulkes North	30%

5.3 Modeling Bursts

A basic GRB light curve will contain an initial power-law decay, followed by a jet break to a steeper power-law decay. This behavior can be modeled by Equation 4.2.

However, often the jet break from one power-law decay to another is too weak to detect. Therefore, for a simplistic GRB model light curve, a single power-law will serve our purposes.

A plot of many well-established GRB light curves is shown in Figure 5.4. This plot will be the basis for our model. A typical light curve (GRB 990123), if extrapolated back to 0.0001 days, begins at an R-band magnitude of 9 (not accounting for prompt emission).

A model burst will be drawn from a random Gaussian distribution centered on an R-band magnitude of 9 with a sigma of 1 magnitude. The slope of the line is α=1.2.

5.4 Simulating Bursts

A burst is modeled using the above characteristics. A random number generator determines the time, right ascension, and declination of our simulated burst, and sends it to the ALT.PRO program, which determines the visibility at the sites of all the telescopes listed in table (Table 5.1). This information is sent to PLOTGRB.PRO (Updike, 2006), which either assumes all telescopes are capable of responding and plots their response accordingly, or employs an algorithm based on their previous response to bursts to attempt to predict whether or not the telescope is likely to respond.

As we saw earlier in our discussion of BATSE, the burst distribution in the sky is isotropic - they originate from no particular direction, and no location is favored over another. Therefore, a random number generator is ideal to simulate the burst coverage.

A sample run of this program is displayed in Figure 5.4. This is the predicted response to GRB 070103, found at RA and DEC. Our program predicts that the following telescopes would have been capable of responding - BOOTES, KAIT, MAO, and Tubitak. Compare this to Figure 5.4, which shows the actual light curves of many recorded bursts.

This program has proved useful in determining who could have observed a burst, especially for consortium writing papers on specific bursts. Since many responding teams

don't bother publishing any data they might have, we can use the program to determine who may have data and who might not.

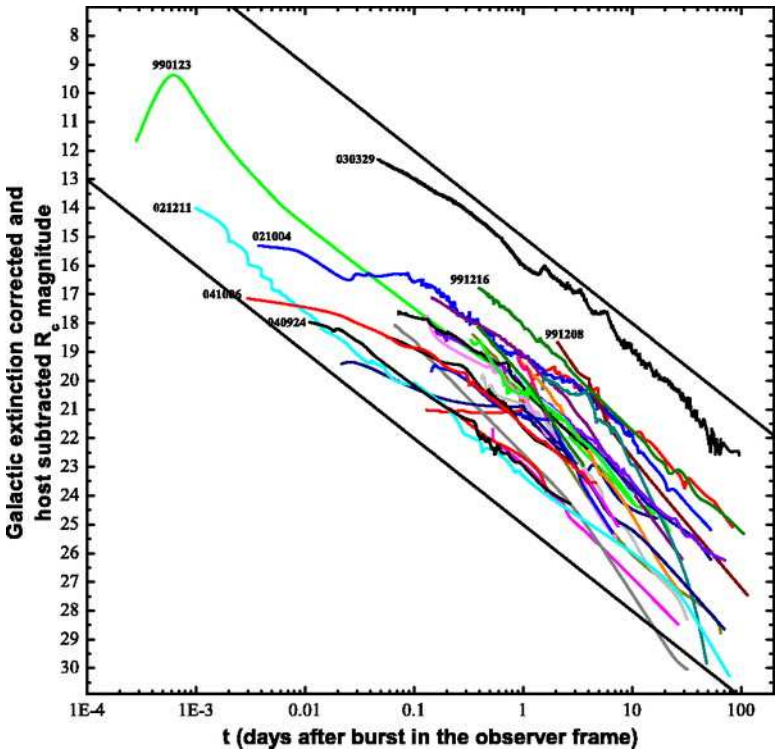

Figure 5.4 Actual light curves of bursts. Kann et al. (2006).

5.4.1 Redshift Dimming

As the redshift of the burst increases, the overall flux we are receiving decreases. However, due to time dilation effects, we are seeing high-z bursts at an earlier time in their evolution, and thus the dimming effects are not as great as we would expect based on the distance alone.

In Figure 5.2, we see the effects detailed above, as well as the 'drop-out' of the bluer bands due to the extinguishing effect of the Lyman alpha forest due to the distribution of neutral hydrogen in the universe. The solid and dotted lines refer to two different models of the neutral hydrogen distribution; they give similar results.

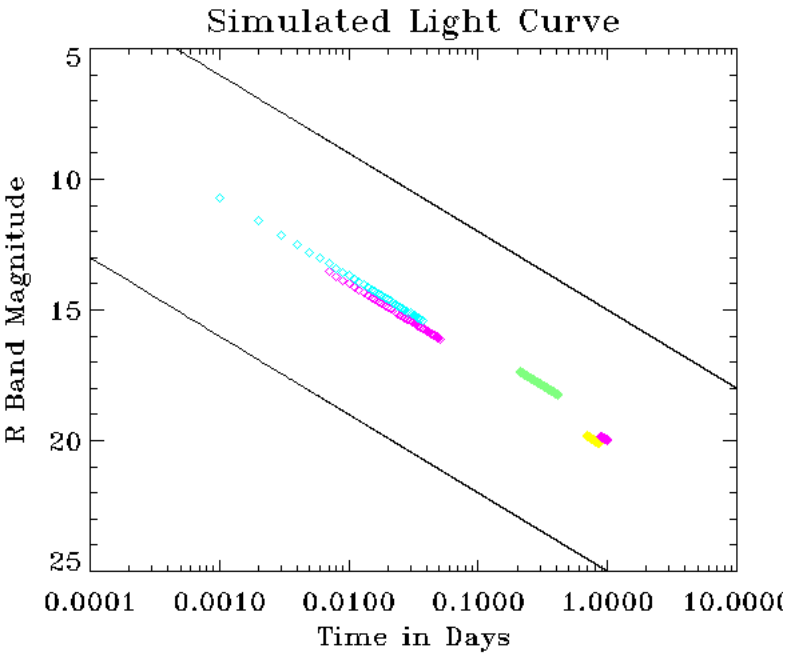

Figure 5.5 Simulated light curve predicting the response to GRB 070103. The four predicted telescopes to respond were BOOTES in blue, KAIT in green, MAO in yellow, and Tubitak in purple. The light curves they could contribute are slightly offset artificially.

As bursts are shifted to higher and higher redshifts, they become increasingly hard to detect. As the redshift increases, we see a significant decrease in the number of visible afterglows, even for large telescopes.

5.5 Further Refinements

This set of programs is a simple model of how the global community will respond to a burst. However, there are many other considerations to take into account.

First, the nature of the burst itself must be considered. Our simulations assume a simple power-law decay, which we know is not the case. The bursts often exhibit flares, re-brightening periods, and jet-breaks, all of which will change the results, but slightly.

Second, we made no attempt to account for telescope availability. While the smaller robotic telescopes are dedicated instruments, the larger telescopes (e.g., Keck, VLT, Tautenburg-Schmidt) run on scheduled time or target of opportunity observations. Therefore, although

these instruments may be capable of detecting the burst, they cannot be relied upon to observe it.

Third, instrument problems and weather conditions at the sites were not taken into account. Although we could estimate how many clear nights a year a site may get, we do not have a way of estimating how often a telescope will encounter problems that may prevent it from observing a GRB.

Fourth, we know that simply getting our response information from the GCNs is not the most accurate tool. Many teams may observe a burst and not report on it - either to reserve their data for a paper, or because similar observations (or more conclusive observations) have already been reported, making theirs redundant.

Fifth, it will prove useful to eventually include all telescopes that have ever responded to a GRB.

Sixth, we hope to eventually make this program a web-based utility for all users looking for an airmass/altitude chart. Current web-based utilities are text-based, and our program presents a clear plot, with the option of plotting multiple objects.

5.6 Conclusions

It is clear the the future of GRB follow-up will be in the infrared. It is therefore crucial to begin planning for a more comprehensive IR follow-up program, as well as finding more dedicated instruments capable of responding out to high magnitudes to continue ground-based support of the larger number of GRB detections we anticipate coming from the GLAST and EXIST missions.

CHAPTER 6
CONCLUSIONS

Gamma ray bursts still remain somewhat a mystery, even after 40 years of observations. Understanding the energy output and distribution, the jet morphology, the supernova mechanisms, and the surrounding medium will greatly improve our understanding of GRBs. Observational campaigns in multiple wavelengths will add to the overall understanding of bursts.

We observed GRB 070125 with the SARA telescope, and, with the help of our collaboration, we put together a light curve in the R-band for this burst. We measured a jet break time of 3.5 days, and, using the published redshift (corresponding to a lookback time of approximately 10 billion years), we calculated a total energy output of 1.67×10^{51} ergs. Using a late-time observation done at the LBT, we conclude that the GRB host galaxy has a absolute luminosity of -17.9, which is consistent with the current knowledge of GRB host galaxies.

In addition, upcoming missions will provide us with many more bursts to study. Continued ground-based support for these missions is crucial, as is near-IR coverage. Our global response program is capable of simulating the response to bursts and reporting on 'gaps' in the system - possible burst locations that are not promptly observable by ground-based follow-up instruments. This may prove useful in assisting the *Swift* mission in planning where the satellite will be looking on a given night. We stress the need for more NIR coverage and a larger number of dedicated instruments.

BIBLIOGRAPHY

Akerlof, C., Balsano, R., Barthelmy, S., Bloch, J., Butterworth, P., Casperson, D., Cline, T., Fletcher, S., Frontera, F., Gisler, G., Heise, J., Hills, J., Kehoe, R., Lee, B., Marshall, S., McKay, T., Miller, R., Piro, L., Priedhorsky, W., Szymanski, J., & Wren, J. 1999, Nature, 398, 400

Amati, L. 2005, Nuovo Cimento C Geophysics Space Physics C, 28, 251

Bellm, E., Bandstra, M., Boggs, S., Wigger, C., Hajdas, W., Smith, D. M., & Hurley, K. 2007, GRB Coordinates Network, 6025, 1

Beuermann, K., Hessman, F. V., Reinsch, K., Nicklas, H., Vreeswijk, P. M., Galama, T. J., Rol, E., van Paradijs, J., Kouveliotou, C., Frontera, F., Masetti, N., Palazzi, E., & Pian, E. 1999, A&A, 352, L26

Bloom, J. S., Kulkarni, S. R., Djorgovski, S. G., Eichelberger, A. C., Côté, P., Blakeslee, J. P., Odewahn, S. C., Harrison, F. A., Frail, D. A., Filippenko, A. V., Leonard, D. C., Riess, A. G., Spinrad, H., Stern, D., Bunker, A., Dey, A., Grossan, B., Perlmutter, S., Knop, R. A., Hook, I. M., & Feroci, M. 1999, Nature, 401, 453

Bloom, J. S., Starr, D., & Blake, C. H. 2007, GRB Coordinates Network, 6054, 1

Cenko, S. B. & Fox, D. B. 2007, GRB Coordinates Network, 6028, 1

Devillard, N. 1999, in ASP Conf. Ser. 172: Astronomical Data Analysis Software and Systems VIII, ed. D. M. Mehringer, R. L. Plante, & D. A. Roberts, 333–+

Durig, D. T. 2007, GRB Coordinates Network, 6051, 1

Fishman, G. J. & Meegan, C. A. 1995, ARA&A, 33, 415

Fox, D. B., Berger, E., Price, P. A., & Cenko, S. B. 2007, GRB Coordinates Network, 6071, 1

Frail, D. A., Kulkarni, S. R., Sari, R., Djorgovski, S. G., Bloom, J. S., Galama, T. J., Reichart, D. E., Berger, E., Harrison, F. A., Price, P. A., Yost, S. A., Diercks, A., Goodrich, R. W., & Chaffee, F. 2001, Astrophys. J. Lett., 562, L55

Fruchter, A. S., Thorsett, S. E., Metzger, M. R., Sahu, K. C., Petro, L., Livio, M., Ferguson, H., Pian, E., Hogg, D. W., Galama, T., Gull, T. R., Kouveliotou, C., Macchetto, D., van Paradijs, J., Pedersen, H., & Smette, A. 1999, Astrophys. J. Lett., 519, L13

Fynbo, J. P. U., Watson, D., Thöne, C. C., Sollerman, J., Bloom, J. S., Davis, T. M., Hjorth, J., Jakobsson, P., Jørgensen, U. G., Graham, J. F., Fruchter, A. S., Bersier, D., Kewley, L., Cassan, A., Castro Cerón, J. M., Foley, S., Gorosabel, J., Hinse, T. C., Horne, K. D., Jensen, B. L., Klose, S., Kocevski, D., Marquette, J.-B., Perley, D., Ramirez-Ruiz, E., Stritzinger, M. D., Vreeswijk, P. M., Wijers, R. A. M., Woller, K. G., Xu, D., & Zub, M. 2006, Nature, 444, 1047

Garnavich, P., Fan, X., Jiang, L., Dai, X., Kuhn, O., Bouche, N., Buschkamp, P., Smith, P., Milne, P., Bechtold, J., Stanek, K. Z., Prieto, J., Wagner, R. M., Rhoads, J., Hill, J., Baruffolo, A., Desantis, C., Diolaiti, E., Dipaola, A., Farinato, J., Fontana, A., Gallozzi, S., Gasparo, F., Giallongo, E., Grazian, A., Pasian, F., Pedichini, F., Ragazzoni, R., Smareglia, R., Speziali, R., Testa, V., & Vernet, E. 2007, GRB Coordinates Network, 6165, 1

Greco, G., Terra, F., Bartolini, C., Guarnieri, A., Piccioni, A., Pizzichini, G., Nanni, D., Gualandi, R., & Polcaro, V. F. 2007, GRB Coordinates Network, 6047, 1

Guetta, D., Spada, M., & Waxman, E. 2001, Astrophys. J., 557, 399

Haislip, J., Reichart, D., Lacluyze, A., Ivarsen, K., Nysewander, M., Foster, A., & Crain, J. A. 2007, GRB Coordinates Network, 6044, 1

Haislip, J. B., Nysewander, M. C., Reichart, D. E., Levan, A., Tanvir, N., Cenko, S. B., Fox, D. B., Price, P. A., Castro-Tirado, A. J., Gorosabel, J., Evans, C. R., Figueredo, E., MacLeod, C. L., Kirschbrown, J. R., Jelinek, M., Guziy, S., Postigo, A. D. U., Cypriano, E. S., Lacluyze, A., Graham, J., Priddey, R., Chapman, R., Rhoads, J., Fruchter, A. S., Lamb, D. Q., Kouveliotou, C., Wijers, R. A. M. J., Bayliss, M. B., Schmidt, B. P., Soderberg, A. M., Kulkarni, S. R., Harrison, F. A., Moon, D. S., Gal-Yam, A., Kasliwal, M. M., Hudec, R., Vitek, S., Kubanek, P., Crain, J. A., Foster, A. C., Clemens, J. C., Bartelme, J. W., Canterna, R., Hartmann, D. H., Henden, A. A., Klose, S., Park, H.-S., Williams, G. G., Rol, E., O'Brien, P., Bersier, D., Prada, F., Pizarro, S., Maturana, D., Ugarte, P., Alvarez, A., Fernandez, A. J. M., Jarvis, M. J., Moles, M., Alfaro, E., Ivarsen, K. M., Kumar, N. D., Mack, C. E., Zdarowicz, C. M., Gehrels, N., Barthelmy, S., & Burrows, D. N. 2006, Nature, 440, 181

Hurley, K., Cline, T., Mitrofanov, I., Kozyrev, A., Litvak, M., Sanin, A., Tret'yakov, V., Parshukov, A., Boynton, W., Fellows, C., Harshman, K., Shinohara, C., Starr, R., Yamaoka, K., Ohno, M., Fukazawa, Y., Takahashi, T., Tashiro, M., Terada, Y., Murakami, T., Makishima, K., Smith, D. M., Lin, R. P., McTiernan, J., Schwartz, R., Wigger, C., Hajdas, W., Zehnder, A., von Kienlin, A., Lichti, G., Rau, A., Cummings, J., Krimm, H., Barthelmy, S., & Gehrels, N. 2007, GRB Coordinates Network, 6024, 1

Kann, D. A., Klose, S., & Zeh, A. 2006, Astrophys. J., 641, 993

Kouveliotou, C., Meegan, C. A., Fishman, G. J., Bhat, N. P., Briggs, M. S., Koshut, T. M., Paciesas, W. S., & Pendleton, G. N. 1993, Astrophys. J. Lett., 413, L101

Lamb, D. Q. & Reichart, D. E. 2001, ArXiv Astrophysics e-prints

MacFadyen, A. I., Woosley, S. E., & Heger, A. 2001, Astrophys. J., 550, 410

Marshall, F. E. & Racusin, J. 2007, GRB Coordinates Network, 6036, 1

Matt, S. & Pudritz, R. E. 2005, Astrophys. J. Lett., 632, L135

Meegan, C. A., Fishman, G. J., Wilson, R. B., Horack, J. M., Brock, M. N., Paciesas, W. S., Pendleton, G. N., & Kouveliotou, C. 1992, Nature, 355, 143

Meegan, C. A., Pendleton, G. N., Briggs, M. S., Kouveliotou, C., Koshut, T. M., Lestrade, J. P., Paciesas, W. S., McCollough, M. L., Brainerd, J. J., Horack, J. M., Hakkila, J., Henze, W., Preece, R. D., Mallozzi, R. S., & Fishman, G. J. 1996, Astrophys. J. Suppl., 106, 65

Melchiorri, A. & Ödman, C. J. 2003, Phys. Rev. D, 67, 081302

Prochaska, J. X., Foley, R., Perley, D., & Steele, T. 2007a, GRB Coordinates Network, 6031, 1

Prochaska, J. X., Roelofs, G., Bloom, J., & Steeghs, D. 2007b, GRB Coordinates Network, 6032, 1

Reichart, D. E. 1998, Astrophys. J. Lett., 495, L99+

Rhoads, J. E. 1997, Astrophys. J. Lett., 487, L1+

Sari, R., Piran, T., & Halpern, J. P. 1999, Astrophys. J. Lett., 519, L17

Stanek, K. Z., Matheson, T., Garnavich, P. M., Martini, P., Berlind, P., Caldwell, N., Challis, P., Brown, W. R., Schild, R., Krisciunas, K., Calkins, M. L., Lee, J. C., Hathi, N., Jansen, R. A., Windhorst, R., Echevarria, L., Eisenstein, D. J., Pindor, B., Olszewski, E. W., Harding, P., Holland, S. T., & Bersier, D. 2003, Astrophys. J. Lett., 591, L17

Uemura, M., Arai, A., & Uehara, T. 2007, GRB Coordinates Network, 6039, 1

Updike, A. C., Hartmann, D. H., Bryngelson, G. L., Goldthwaite, R. C., & Puls, J. R. 2007a, GRB Coordinates Network, 6029, 1

Updike, A. C., Hartmann, D. H., King, J. R., & Brittain, S. D. 2006, in American Astronomical Society Meeting Abstracts, 212.06–+

Updike, A. C., Hartmann, D. H., Klose, S., & Fruchter, A. 2007b, GRB Coordinates Network, 5994, 1

Wijers, R. A. M. J., Rees, M. J., & Meszaros, P. 1997, MNRAS, 288, L51

Wolf, C. & Podsiadlowski, P. 2007, MNRAS, 375, 1049

Woosley, S. E. 1993, in Bulletin of the American Astronomical Society, Vol. 25, Bulletin of the American Astronomical Society, 894–+

Xing, L. P., Zhai, M., Qiu, Y. L., Wei, J. Y., Hu, J. Y., Deng, J. S., Urata, Y., & Zheng, W. K. 2007, GRB Coordinates Network, 6035, 1

Yoshida, M., Yanagisawa, K., & Kawai, N. 2007, GRB Coordinates Network, 6050, 1